# Mechanism of the Hydrogen Evolution Reaction in Mildly Acidic Environments on Gold

**Aria Kahyarian,*,z Bruce Brown, and Srdjan Nesic**

*Institute for Corrosion and Multiphase Flow Technology, Department of Chemical and Biomolecular Engineering, Ohio University, Athens, Ohio 45701, USA*

Despite numerous studies investigating the kinetics of the hydrogen evolution reaction (HER) on a gold surface in acidic solutions, the underlying mechanism of this reaction have remained controversial to date. In the present study, the existing mechanisms are reevaluated and found to be inadequate in explaining the steady state polarization behavior of the hydrogen evolution reaction in an extended cathodic potentials and mildly acidic pH range. It was shown that a mechanism including a surface diffusion step of $H_{ads}$ alongside the Volmer, Heyrovsky, and Tafel elementary steps, best describes the experimental data obtained in acidic perchlorate solutions up to pH 5, while the rate determining step changes both with pH and electrode potential. This overall HER mechanism was further verified using a comprehensive mathematical model based on the proposed elementary steps, where a satisfactory agreement with experimental results was obtained.



Manuscript submitted December 2, 2016; revised manuscript received March 14, 2017. Published April 6, 2017. This was Paper 927 presented at San Diego, California, Meeting of the Society, May 29- June 2, 2016.

The hydrogen evolution reaction (HER) has been the subject of numerous studies, either as a platform for investigating the theory of electrochemical processes,[1–9] or in terms of hydrogen production, energy storage, and energy conversion,[10–12] due to its significance in the alternative energy source framework. This trend had also include extensive investigations of the mechanism of the HER on gold in acidic solutions.[6,8,13–21] However, a literature survey shows no general agreement on the underlying mechanism of this reaction to date.[13–15,17,18,20,21] Besides, the majority of the proposed mechanisms have been developed based on experimental results obtained in highly acidic environments,[6,8,13–21] but were not examined over an extended pH range.

The experimental polarization curves obtained on gold in acidic solutions repeatedly reported to have two distinct Tafel slopes with values in the range of 50–70 mV at lower current densities and 100–130 mV at higher current densities.[3,6,16,18,21,22] A number of different explanations for the underlying mechanism based on these observed Tafel slopes have been proposed in the literature. In a study by Ives[20] in 0.1 N HCl solutions, the author reported polarization curves with an uncharacterized region at low current densities preceding to the 120 mV Tafel slope range. That uncharacterized section of the voltammograms had a significantly lower Tafel slope with values about 50–70 mV, which was extended to the cathodic currents up to about 1 $A.m^{-2}$ and overpotentials up to about 150 mV. The author associated this lower Tafel slope with the interference of the hydrogen oxidation reaction.[20] However, considering the experimental conditions in that study, no significant interference of anodic currents due to hydrogen gas oxidation is expected, especially at the cathodic overpotentials as high as 150 mV.

Bockris et al.[14,23] suggested that the apparent change of Tafel slope to ~60 mV was caused by the change in potential drop across the diffusion double layer. This effect was believed to be most profound at the potentials near the potential of zero charge (PZC). Therefore, authors suggested that for the mechanism with theoretical Tafel slope of ~120 mV (2.3RT/βF), lower apparent Tafel slopes with a minimum of ~60 mV can be observed in the vicinity of PZC. At the potentials notably different from the PZC, this effect becomes insignificant, thus the apparent Tafel slope tends to reach the theoretical value (~120 mV). However, as suggested elsewhere,[18,24] the reported PZC of gold[25,26] is significantly higher than the potentials at which the change in the Tafel slope occurs experimentally.

Another mechanism based on the barrierless discharge of $H^+$ was also proposed to explain the observed ~60 mV Tafel slope.[13,21] Khanova and Krishtalik[13] suggest that barrierless discharge is feasible on a gold surface at significantly low overpotentials. This means that the activation energy of the HER is equal to its Gibbs free energy change and thus, the symmetry factor of the reaction is unity. Considering the Tafel slope of 2.3RT/βF for the Volmer step, the observed value is therefore ~60 mV. The transition to 120 mV Tafel slope was then associated with the change to ordinary discharge with $\beta = 1/2$.[13,21] Considering the rate determining Volmer reaction throughout the full range of cathodic currents, either as an ordinary charge transfer reaction or a barrierless reaction, the surface coverage of $H_{ads}$ is expected to be low ($\theta \rightarrow 0$), as discussed in more detail in $H^+$ adsorption rate determining step section below. However, this was found to be in contrast with the findings from a study by Chun et al.[6] where a significant coverage of $H_{ads}$ ($\theta \rightarrow 1$) was reported in the 120 mV Tafel slope region.

The surface diffusion limiting step has also been suggested as a possible mechanism for the observed lower Tafel slope.[15,17,23] This proposed mechanism states that the hydrogen ion discharge (adsorption) sites are different from desorption sites and the surface diffusion of the adsorbed hydrogen atoms between these sites is the limiting step in the overall HER rate. Brug et al.[15] suggested that desorption sites (surface defects such as impurities) are kinetically favored reaction sites compared to the gold itself and govern the overall reaction rate. The rate of reaction was therefore, limited by the surface diffusion of adsorbed hydrogen atoms to these reaction sites. Nevertheless, the similar behavior of Tafel slopes observed for high purity electrodes (99.99 wt% in the present study and other studies such as the one by Perez et al.[16]) suggest that the effect of impurities may have been overemphasized.

Conway and Bai[17] also suggested a similar rate determining mechanism involving surface diffusion. However, these authors argued that the adsorption/discharge sites were not suitable for desorption due to the interference by the strong adsorption of anions present in the electrolyte ($HSO_4^-$ and $SO_4^-$ in that study). Hence, the following mechanism was proposed where the second step represents the surface diffusion of $H_{ads}$. However, their proposed mechanism also fails to address the increased Tafel slope at high current densities (~120 mV).

$$H^+ + e^- \rightleftharpoons H_{ads,A}$$

$$H_{ads,A} \rightarrow H_{ads,B}$$

$$H_{ads,B} + H^+ + e^- \rightarrow H_2$$

Brug et al.[15] discussed the mechanism of the HER in the context of conventional Volmer-Heyrovsky-Tafel elementary steps. The authors

*Electrochemical Society Student Member.
zE-mail: ak702711@ohio.edu

proposed a mechanism with Tafel reaction being the rate determining step in the 60 mV Tafel slope region and a shift to Heyrovsky reaction being the rate determining step in the 120 mV Tafel slope region.

As discussed above, the majority of previously proposed mechanisms fail to fully address the polarization behavior of the HER as observed in the experimental results. The mechanism based on the conventional elementary steps proposed by Brug et al.[15] can be considered further as a possibility. Another mechanism including a surface diffusion step (Conway and Bai[17]) also appears to be able to explain the observed features of the polarization curves, given that some modification are introduced to address the increase of the Tafel slope. The goal of the present paper is to reevaluate these two mechanisms over an extended pH and potential range, discuss the conditions at which these mechanisms are valid, and finally, settle on a mechanism that agrees best with polarization behavior of the HER on a gold surface for the conditions in the present study as well as those previously reported in the literature.

It is worth mentioning that the mildly acidic and near-neutral solutions are of special interest in the aqueous corrosion of steel, which is commonly encountered in industrial applications.[27–31] To date, most of the mechanistic corrosion rate predictive models[30–33] base the calculation of the cathodic current (rate of the HER) on studies[14,34,35] where the experimental conditions were significantly different from those encountered in the models' targeted applications. Considering the profound effect of pH,[36,37] electrode material and surface structure,[15,23,34,38,39] overpotential,[40] and solution composition[37] on the kinetics of the HER, a comprehensive understanding of the reaction mechanism and its kinetics is essential for accurate modeling of such systems.

## Methodology

***Experimental procedures.—***The experiments were carried out in a 1 L glass cell with a conventional three electrode arrangement. A silver/silver chloride reference electrode was connected to the glass cell through a Luggin capillary filled with 1 M potassium chloride solution. A graphite rod, 5 mm in diameter and 15 cm in length, was used as the counter electrode, which was placed in a separate glass tube with a fine fritted glass connection at the bottom. A 99.99 wt% polycrystalline gold rotating disk electrode (Pine instruments) with a 5 mm diameter was used as the working electrode. The electrode was polished with 0.05 μm silicon suspension, rinsed and sonicated for 5 minutes using deionized water and subsequently with isopropanol, prior to each test. The working electrode was further electrochemically cleaned in the studied solution with 10 consecutive potential cycles, from −0.6 V to 0.8 V (vs. Ag/AgCl) at 100 $mV.s^{-1}$ until a steady voltammogram was achieved (typically after 7 cycles). Finally, the electrode was left at open circuit potential for 5 minutes before starting each potential sweep. The rotation speed of the working electrode was fixed at 2000 rpm throughout the electrochemical measurements. The steady state voltammograms reported in the present study were obtained at 0.1 $mV.s^{-1}$ scan rate using a 2 $s^{-1}$ sampling period, by sweeping the potential from the OCP toward more negative values. The polarization curves were further corrected for ohmic drop using the solution resistance obtained from electrochemical impedance measurements performed after each potential sweep.

The supporting electrolyte was 0.1 M solution of analytical grade sodium perchlorate in deionized water. The solution temperature was maintained at 30.0 ± 0.5°C. The pH was adjusted by addition of a diluted perchloric acid solution, as required. Then, the electrolyte was deaerated for at least 90 minutes using nitrogen gas, and the outlet gas was monitored with an oxygen sensor (Orbisphere 410). Maximum dissolved oxygen content before initiating the experiment was 3 ppb (typically below 1 ppb). During the electrochemical measurements, the purging was stopped and the solution was blanketed with nitrogen gas.

***Numerical methods.—****Parametric study* calculations were performed using MATLAB 2012 software. The partial derivatives were numerically calculated at a fixed pH and potential, by using a two-point finite difference approximation, $f' = (f(x+h)-f(x))/h$, with $h = 0.001$ for both pH and potential. The values of $f(x)$ and $f(x+h)$ were obtained based on the known θ values. By repeating this procedure and varying the characteristic adsorption parameters, a map of theoretical kinetic parameters was be obtained.

*Mathematical model* of the system was developed by numerical solution of a set of differential equations, as discussed in Mathematical model section. The following set of dimensionless variables were defined to replace distance ($x$), concentration ($C_i$), and potential ($E$ and $\phi$).

$$\zeta = \frac{x}{\delta} \quad \xi_i = \frac{C_i}{C_i^b} \quad \Phi = \frac{F\phi}{RT} \quad \psi = \frac{FE}{RT}$$

The resulting set of differential equations was solved by the finite difference method. The first and second order central difference approximations were used to discretize the first order and the second order derivatives appearing in the governing equation, respectively. The metal/solution interface boundary condition was discretized using first order three point forward approximation. The coefficient matrix of the discretized equations was then formed and solved using Newman's "BAND" method, which is described in detail elsewhere.[58,59] The calculations were performed with 200 spatial nodes and a maximum cumulative error of $R^2 = 10^{-12}$ for all iterations. The source code of the model was developed using Microsoft Visual Studio 2012 and an Intel Visual Fortran Compiler 13.0. Furthermore, a graphic user interface was developed, using MATLAB 2012 GUI, in order to simplify input/output operations.

## Results and Discussion

***Experimental results.—***The steady state voltammograms of the HER obtained on a gold electrode, at the experimental conditions described in Methodology section, are shown in Figure 1. The polarization curves obtained at pH 4 and pH 5 showed a similar behavior. That is, a linear increase of the current density at less negative potentials, which is associated with hydrogen evolution from $H^+$ ions, followed by a plateau that is a result of mass transfer limitation of $H^+$ ions, and another linear increase at more negative potentials due to the hydrogen evolution from water. At lower pH values (2 and 3) the mass transfer limiting current and the water reduction line were not observed as they exceeded the maximum measurable current densities (~40 $A.m^{-2}$). The maximum measureable current density limit was imposed by the blockage effect resulting from hydrogen gas accumulation at the electrode surface. The current densities at which a significant blockage effect was observed is affected by the sweeping

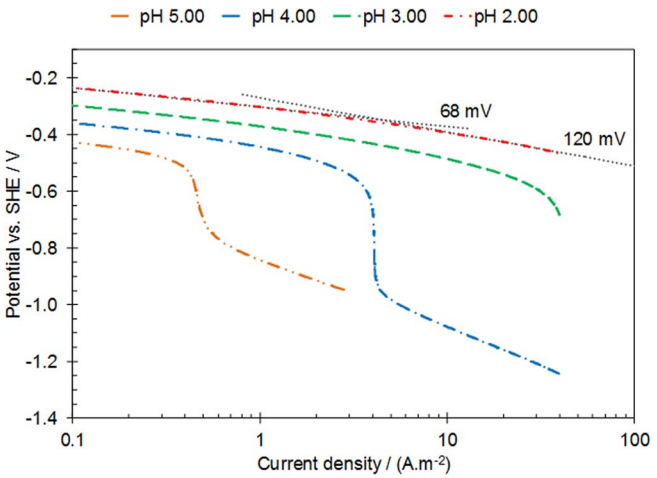


**Figure 1.** Steady state voltammograms of the HER on gold RDE at 2000 rpm, 30°C and 0.1 M $NaClO_4$.

**Table I. Literature survey for experimental Tafel slope of HER on gold in acidic solutions.**

| Electrolyte | Lower b (mV) | Higher b (mV) | Reference |
|---|---|---|---|
| 0.1 M $HClO_4$ | 60 | 120 | 16 |
| 0.1 N HCl | 71 | 97 | 14 |
| 0.01, 0.001 N HCl | 72 and 84 | - | |
| 0.5 M $H_2SO_4$ | 60 | - | 17 |
| 0.1 M and 0.01 M $HClO_4$ | 50 to 70 | - | 64 |
| 1 M $H_2SO_4$ | 30 | 110 | 18 |
| 1 M $HClO_4$ | 62 to 97 | 118 | 15 |
| 1 M and 0.1 M $H_2SO_4$ | 53 to 69 | 105 to 141 | 13 |
| 0.5 M $H_2SO_4$ | 30 | - | 6 |
| 1 N HCl | 60 | - | 19 |
| 0.03 M $HClO_4$ | 60 | 120 | 21 |

rate of the produced hydrogen gas i.e. the flow velocity parallel to the electrode surface. At 2000 rpm rotation rate used throughout this study, no significant accumulation of hydrogen gas was observed at the current densities below 40 $A.m^{-2}$.

The present study is focused on the polarization behavior associated with the $H^+$ ion reduction reaction at the current densities below the mass transfer limiting current, which was observed for all pH values as shown in Figure 1. In this range, at low current densities (below 4 $A.m^{-2}$), Tafel slopes in the range of 68 ± 5 mV were observed throughout the studied pH range. Although, at pH 5 the slope of the polarization curve appears to have slightly increased due to mass transfer limitation interference. At higher current densities (above 4 $A.m^{-2}$) the Tafel slope increased to 120 ± 2 mV, which was most clearly observed at pH 2.

The experimental Tafel slopes obtained in the present study were found to agree well with the results reported in the literature. As summarized in Table I, the observation of two distinctive Tafel slopes for the HER on gold has been frequently reported in the literature. The lower Tafel slope was generally reported within the range of 50 mV to 70 mV. At higher current densities, the reported Tafel slopes were in the range of 100 mV to 130 mV. In the studies reporting a single Tafel slope, the values obtained were generally within the 50 mV to 70 mV Tafel slope range.

In addition to the Tafel slope, the reaction order of the HER with respect to the concentration of hydrogen ions is also a characteristic kinetic parameter that can provide additional information about the underlying mechanism. Figure 2 presents the pH dependence

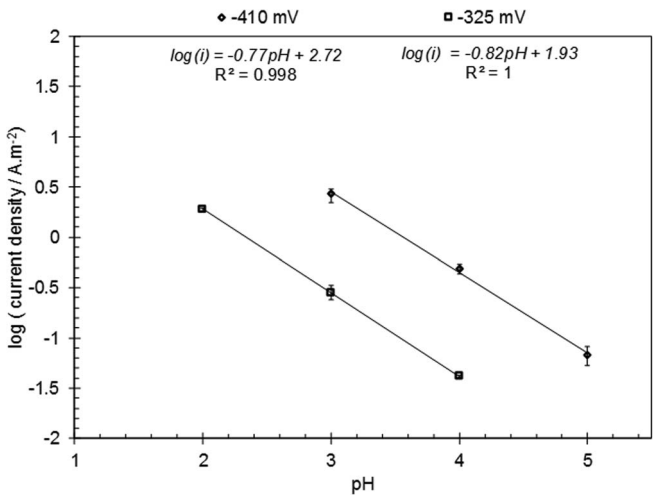


**Figure 2.** pH dependence of current density at −0.410 V (vs. SHE) and −0.325 V (vs. SHE) at 2000 rpm, 30°C and 0.1 M $NaClO_4$. Error bars show the standard deviation from minimum of three repetitions. The equation of each trendline is shown under the corresponding legend.

of the current density at two fixed potentials for the experimental data obtained in the present study. In this graph (log(i) vs. pH), the slope of the trendline represents the apparent reaction order of HER ($-p_{(H+)}$) which was found to be approximately 0.8 at the pH range from 2 to 5, while some variation at different potentials and pH values was observed. The observed value of the apparent reaction order and its variation with pH and potential may imply a multi-step reaction mechanism and possibly multiple reaction pathways, which is not unexpected for acidic hydrogen evolution reaction. The values for reaction order were not frequently reported in the literature, however, in studies by Kuhn and Byrne[18] and by Brug et al.,[15] the reaction order of 1 with significant deviations with potential were reported.

***Parametric study of the HER mechanisms.***—The hydrogen evolution reaction is conventionally described by the sequence of three elementary steps as shown via Reaction 1 to Reaction 3.[41] These reactions are known as the Volmer (electrochemical hydrogen ion adsorption) reaction, Heyrovsky (electrochemical desorption) reaction, and Tafel (chemical desorption) reaction, respectively. In addition to the conventional elementary steps, Reaction 4 below represents the surface diffusion elementary step, similar to what was discussed by Conway and Bai,[17] where A and B are distinct adsorption and desorption sites.

Volumer reaction

$$H^+ + e^- \rightleftharpoons H_{ads} \quad [1]$$

Heyrovsky reaction

$$H^+ + H_{ads} + e^- \rightarrow H_2 \quad [2]$$

Tafel reaction

$$2H_{ads} \rightarrow H_2 \quad [3]$$

Surface diffusion reaction

$$H_{ads,A} \rightarrow H_{ads,B} \quad [4]$$

Here, the hydrogen oxidation reaction is assumed to be insignificant during cathodic polarization. This assumption is in accordance with the experimental procedures described in Methodology section, which were designed to minimize the effect of hydrogen oxidation reaction on the cathodic polarization curves.

The mechanism of the HER are discussed in terms of the kinetic parameters such as Tafel slope and reaction order,[23,37,40,42,43] these parameters are experimentally obtained by measuring the change in the current as a function of potential (Tafel slope) and pH (reaction order). The mechanism of the HER at various conditions is then determined by identifying a reaction sequence with kinetic parameters closest to the experimental values. The kinetic parameters corresponding to any given elementary step (Reaction 1 to Reaction 4) can be calculated based on their corresponding rate equations. The rate of the elementary reactions shown above, can be described by Equation 5 to Equation 8, respectively.[17,44–46]

$$\upsilon_V = k_{f,V}(1-\theta)\left[H^+\right]e^{-\lambda_V u\theta}e^{-\beta_V \frac{FE}{RT}} - k_{b,V}\,\theta e^{(1-\lambda_V)u\theta}e^{(1-\beta_V)\frac{FE}{RT}} \quad [5]$$

$$\upsilon_H = k_{f,H}\left[H^+\right]\theta e^{(1-\lambda_H)u\theta}e^{-\beta_H \frac{FE}{RT}} \quad [6]$$

$$\upsilon_T = k_{f,T}\theta^2 e^{2(1-\lambda_T)u\theta} \quad [7]$$

$$\upsilon_D = k_{f,D}\theta e^{(1-\lambda_D)u\theta} \quad [8]$$

In these equations, $k$ is the reaction rate constant, θ is the surface coverage by adsorbed hydrogen atoms ($H_{ads}$), the first exponential terms describe the interaction of $H_{ads}$ at the surface where $u$ represents the correlation coefficient of the interaction energy, and where present – the second exponential term accounts for the effect of potential. Note that, for the electrochemical Reactions 5 and 6, it can be

**Table II. Theoretical expressions of reaction order and Tafel slope for various elementary steps.**

| | $\frac{1}{b} = -\left(\frac{\partial \log i}{\partial E}\right)_{pH}$ | $p_{(H^+)} = \left(\frac{\partial \log i}{-\partial pH}\right)_E$ |
|---|---|---|
| Heyrovsky reaction | $\frac{\partial \log(\theta e^{(1-\lambda)u\theta})}{\partial E} - \frac{\beta F}{2.303RT}$ | $1 - \frac{\partial \log(\theta e^{(1-\lambda)u\theta})}{\partial pH}$ |
| Tafel reaction | $2\frac{\partial \log(\theta e^{(1-\lambda)u\theta})}{\partial E}$ | $-2\frac{\partial \log(\theta e^{(1-\lambda)u\theta})}{\partial pH}$ |
| Surface diffusion | $\frac{\partial \log(\theta e^{(1-\lambda)u\theta})}{\partial E}$ | $-\frac{\partial \log(\theta e^{(1-\lambda)u\theta})}{\partial pH}$ |

reasonably assumed that the symmetry factors β and (1-λ) are equal. This assumption is based on the fact that both symmetry factors are associated with the change in the Gibbs free energy of the same activated complex.

Based on the aforementioned elementary steps, three scenarios can exist.

a) $H^+$ adsorption rate determining step.
b) $H_{ads}$ desorption rate determining steps.
c) Surface diffusion rate determining step.

The theoretical expression of the Tafel slope ($b$) and reaction order ($p_{(H+)}$) for case (a) are relatively straightforward as discussed in the following section. However, when the desorption step (b) or the surface diffusion step (c) are rate determining, these expressions become nonlinear functions of surface coverage (as shown in Table II) and cannot be solved analytically without introducing additional assumptions.[4,42] An alternative approach used in the present study is the numerical solution of the expressions shown in Table II, where the nonlinear surface coverage functions and derivatives were numerically obtained, as discussed in Methodology section. Using this approach, the behavior of the Tafel slope and reaction order was investigated as a function of the physiochemical parameters representing the state of surface coverage by $H_{ads}$ ($u$ and $K$). In order to uncover the possible mechanisms of the HER in the conditions of the present study, the results were compared with the experimental data.

*$H^+$ adsorption rate determining step.*—In the case where the $H^+$ adsorption step (a) is slower than the other steps, the rate of the HER is governed by the rate of the forward partial of Reaction 1:

$$\upsilon_V = k_{f,V}\,(1-\theta)\left[H^+\right]e^{-\lambda_V r\theta}e^{-\beta_V \frac{FE}{RT}} \qquad [9]$$

In this case, the concentration of $H_{ads}$ can be considered to be negligibly small ($\theta \to 0$), as a result of its consumption in the faster succeeding steps.[4,41,43] Therefore, both linear and exponential surface coverage dependent terms in Equation 9 can be disregarded and the HER rate can be described as:

$$\upsilon_V = k_{f,V}\left[H^+\right]e^{-\beta_V \frac{FE}{RT}} \qquad [10]$$

The reaction rate relationship shown as Equation 10 corresponds to a Tafel slope of ~120 mV at $T = 303^oK$ ($2 \times 2.303RT/F$) and has a reaction order of 1.

*$H_{ads}$ desorption rate determining steps.*—In the case where the $H_{ads}$ desorption steps are rate determining, the surface coverage of $H_{ads}$ may be significant ($\theta > 0$). Here, one may assume that the Volmer reaction is at quasi-equilibrium, as the reaction preceding the rate determining step. Knowing this assumption is only valid if the kinetics of the forward and backward Volmer reaction are much faster than the succeeding step. Using this simplifying assumption, Equation 5 can be restated as Equation 11, resulting in a Frumkin type adsorption isotherm, describing the surface coverage ($\theta$) of $H_{ads}$:

$$\frac{\theta}{(1-\theta)}e^{u\theta} = K\,e^{\left(-\frac{FE}{RT}\right)}\left[H^+\right] \qquad [11]$$

where $K = k_{f,V}/k_{b,V}$. As shown in Figure 3, this equation can be used to study the response of $\theta$ to changes in pH and potential as a function of $u$ and $K$. This can be further used for numerical calculation of the theoretical kinetic parameters associated with the presumed succeeding reaction, as shown in Table II. This approach was implemented for each rate determining step proceeding the Volmer reaction, as discussed in the text below.

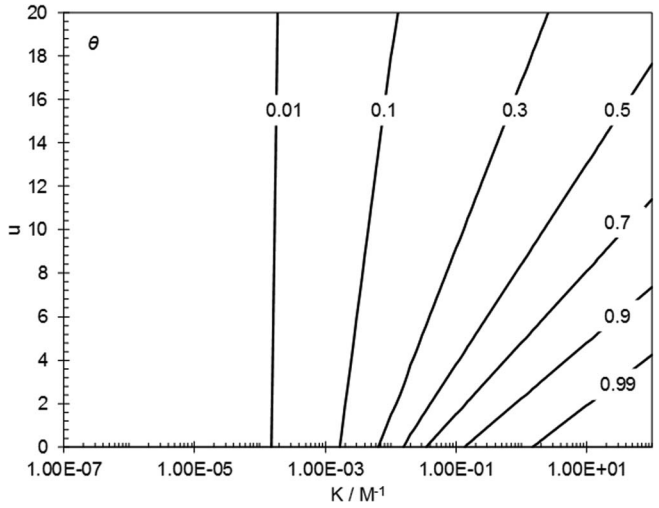


**Figure 3.** Calculated value of the surface coverage of $H_{ads}$ described via Equation 11. At pH 2, −0.230 V (vs. SHE) and 30°C.

*Heyrovsky rate determining step.*—Considering that the Heyrovsky step is rate determining, the Tafel slope and reaction order are shown in Figure 4A and Figure 4B, respectively. These graphs demonstrate a map of these two parameters at a fixed pH and potential while the values of the interaction coefficient ($u$) and the equilibrium constant of the Volmer step ($K$) were varied. That provides a comprehensive view of how Tafel slope and reaction order may change at various conditions. The commonly reported values of Tafel slope and reaction order in literature[4,42,43] are found as limiting conditions in these graphs. As shown in Figure 4A for the Heyrovsky rate determining step, the Tafel slope has the minimum of ~40 mV ($2/3 \times 2.303RT/F$) observed at low values of $K$ ($K < 10^{-5}$ $M^{-1}$), and the maximum of ~118 mV ($2 \times 2.303RT/F$) at high $K$ values ($K > 10^{1}$ $M^{-1}$). At similar conditions, the reaction orders of 2 and 1 were obtained at low and high $K$ values, respectively, as shown in Figure 4B. These two limits for Tafel slope and reaction order were found to correlate with the limiting conditions of the surface coverage shown in Figure 3, where low $K$ values correspond to $\theta \to 0$ and high $K$ values correspond to $\theta \to 1$.

For the two limiting conditions discussed above ($\theta \to 0$ and $\theta \to 1$), as well as for the case when $u$ is negligibly small (along the x-axis in Figure 4A and Figure 4B), Equation 11 can be further simplified. In these conditions, the change in the $\theta$ dependent exponential term in Equation 11 with variation of $\theta$ is negligible when compared to the $\theta$ dependent linear term. Therefore, one can assume that the exponential function is constant, which allows Equation 11 to be reduced to a Langmuir type isotherm. Based on this simplifying assumption, theoretical values of Tafel slope (40 mV and 120 mV) and reaction order (2 and 1, respectively) were obtained in the past studies.[4,15]

On the other hand, when the value of $\theta$ is in-between the limiting conditions described above and $u$ is high, the change in the $\theta$ dependent linear terms with variation of $\theta$ can be assumed to be negligible when compared to the $\theta$ dependent exponential terms. Equation 11 can then be simplified to a Temkin type isotherm and the linear $\theta$ dependent terms of the expressions in Table II may be disregarded.[4] This specifically corresponds to the condition where $\theta = 0.5$ in Figure 3 (when $\theta/(1-\theta) = 1$) with Tafel slope of ~60 mV ($2.303RT/F$) and reaction order of 1.5, as shown in Figure 4A and Figure 4B.

*Tafel rate determining step.*—The results of a similar analysis as described in the previous section are reported in Figure 5 for the case where the Tafel step is rate determining. The Tafel slope is shown in

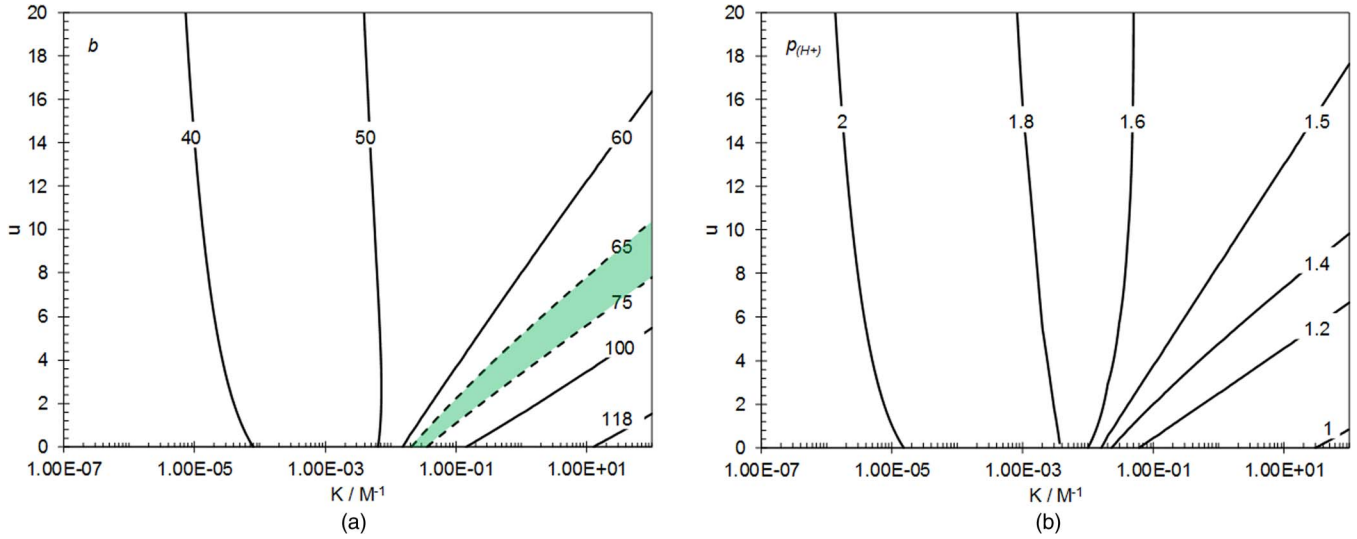


**Figure 4.** Calculated values of the kinetic parameters where the Heyrovsky reaction is the rate determining step. At pH 2, −0.230 V (vs. SHE), 30°C, and $\lambda = 0.5$. A) Tafel slope, and B) reaction order.

Figure 5A where the minimum value of ~30 mV (*1/2 × 2.303RT/F*) was observed at low *K* values (corresponding to $\theta \rightarrow 0$) that increased to infinity at high *K* values (corresponding to $\theta \rightarrow 1$), where Equation 11 can be simplified to a Langmuir type isotherm. As shown in Figure 5B, these Tafel slopes coincide with the reaction order of ~2 and ~0, respectively. At $\theta = 0.5$ where Equation 11 can be simplified to a Temkin type isotherm, the Tafel slope of ~60 mV (*2.303RT/F*) and reaction order of 1 is observed.

*Surface diffusion rate determining step.*—The theoretical values of Tafel slope and reaction order when the surface diffusion is the rate determining step was calculated in a same fashion as described above for other elementary steps, and the results are shown in Figure 6.

Figure 6A shows that the Tafel slope has a minimum value of ~60 mV (*2.303RT/F*) at low *K* values ($K < 10^{-5}$) which corresponds to the reaction order of 1 and $\theta \rightarrow 0$, as shown in Figure 6B and Figure 3, respectively. At high *K* values ($K > 10$), Tafel slope increases to infinity while the reaction order approaches zero and $\theta \rightarrow 1$. At $\theta = 0.5$, where Equation 11 can be simplified to a Temkin type adsorption isotherm, the Tafel slope of ~120 mV (2.303RT/F) and reaction order of 0.5 is obtained.

***Discussion.***—In order to narrow down the possible mechanisms of the HER in the conditions of the present study, the theoretical values of the reaction order and Tafel slope obtained above were further examined, considering the experimentally obtained Tafel slope of 68 ± 5 mV and the reaction order of ~0.8.

Reaction mechanisms including the slow adsorption of $H^+$ step (Volmer reaction) with 120 mV theoretical Tafel slope (as discussed in $H^+$ adsorption rate determining step section) can be readily eliminated, when considering the experimental Tafel slopes of 68 ± 5 mV obtained at low current densities. On the other hand, the Tafel, Heyrovsky, and surface diffusion elementary steps were found to have theoretical Tafel slopes similar to what was observed experimentally, for a certain range of *K* and *u* values. This possibility is illustrated in Figure 4A, Figure 5A, and Figure 6A, as a highlighted area between the dotted lines. However, a Heyrovsky rate determining step may also be eliminated, when considering that in the same range of *u* and *K*, where the Tafel

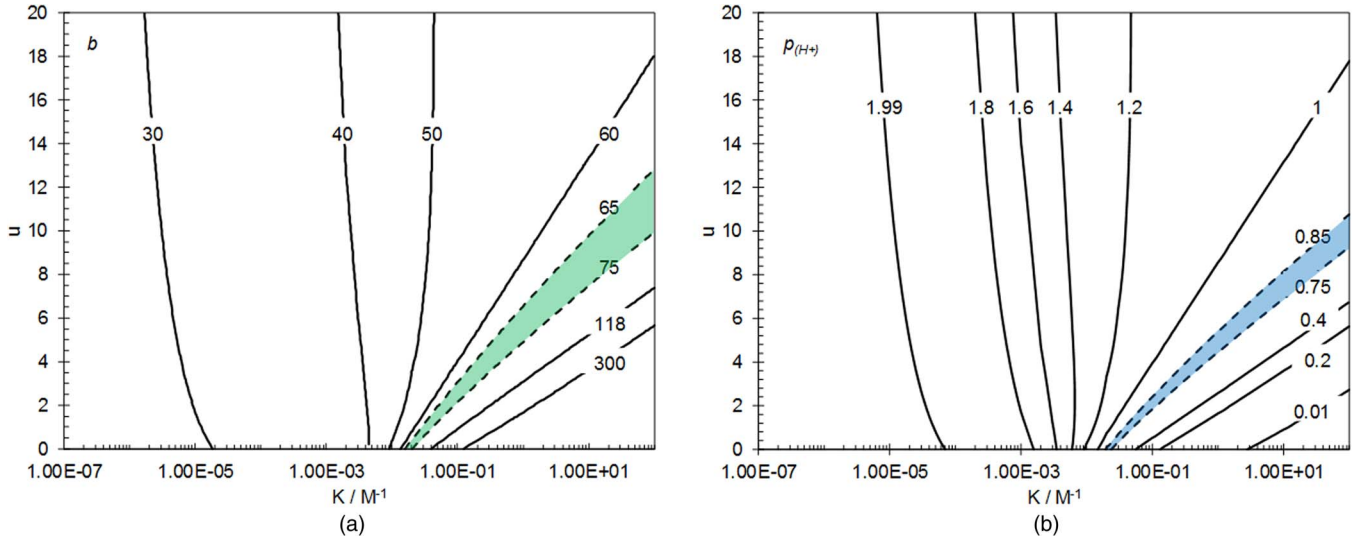


**Figure 5.** Calculated values of the kinetic parameters where the Tafel reaction is the rate determining step. At pH 2, −0.230 V (vs. SHE), 30°C and $\lambda = 0.5$. A) Tafel slope, and B) Reaction order.

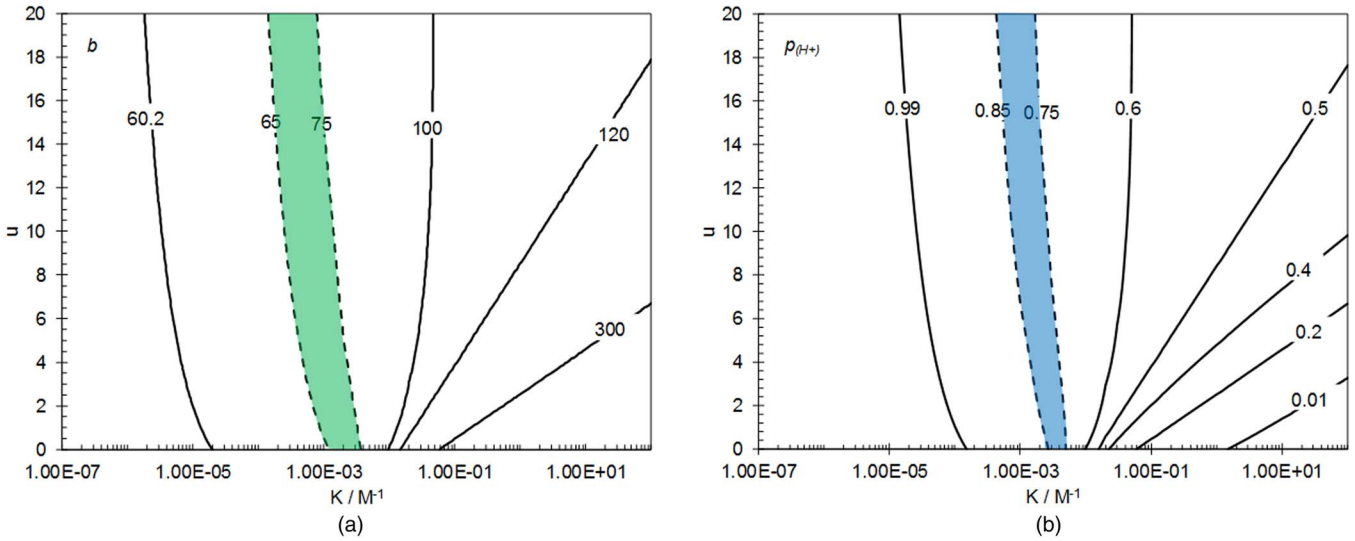


**Figure 6.** Calculated values of the kinetic parameters where the surface diffusion is the rate determining step. At pH 2, −0.230 V (vs. SHE), 30°C and λ = 0.5. A) Tafel slope, and B) Reaction order.

slope is in agreement with experimental data, the reaction orders (shown in Figure 4B) differ significantly.

The reaction orders obtained when the Tafel step or the surface diffusion step were considered to be rate determining (Figure 5B and Figure 6B) suggest that a reasonable agreement with the experimental values can be achieved for both mechanisms. Consequently, at the conditions considered for this parametric study, the rate determining step at lower current densities may be explained through either of following scenarios:

a) a Tafel rate determining step when $0.5<\theta<0.8$.
b) a surface diffusion rate determining step when $\theta \rightarrow 0$.

The possible mechanism underlying the ∼120 mV Tafel slope, observed at higher current densities, can be analyzed in a similar fashion. Considering the discussion in Parametric study of the HER mechanisms section and the possible mechanisms at low current densities, the only scenario with a reasonable agreement to the experimental data is the Heyrovsky reaction being rate determining and $\theta \rightarrow 1$. That results in a theoretical Tafel slope of ∼120 mV and reaction order of 1, as shown in Figure 4A and Figure 4B, respectively.

In the above parametric study, the possible mechanism at the higher current densities (the region with ∼120 mV Tafel slope) was narrowed down to a unique scenario – Heyrovsky rate determining step. However, at the lower current densities (the region with ∼60 mV Tafel slope), the same type of analysis was not able to differentiate between the two possible mechanisms. The main difference between these two mechanisms was in the extent of the surface coverage (θ) by $H_{ads}$. The mechanism having the Tafel reaction as the rate determining step requires a high surface coverage and strong repulsive interaction of $H_{ads}$, whereas, the surface diffusion limiting step suggests a negligible coverage by $H_{ads}$. This can be used as a distinguishing argument between these two mechanisms.

The measurements reported by Brug et al.[15] and Conway and Bai[17] showed that over the low cathodic overpotentials (in the ∼60 mV Tafel slope range) there is no significant adsorption pseudo-capacitance, claiming a negligible coverage by $H_{ads}$. However, before taking these studies in favor of the surface diffusion mechanism, one should also consider the low adsorption capacity of gold surfaces. Let us recall that θ is a relative parameter which is defined as concentration (number) of $H_{ads}$ divided by the maximum concentration of $H_{ads}$ (i.e. number of active sites for $H_{ads}$). However, the number of active sites depends on the nature of the metal surface. For example in a study by Bus and van Bokhoven[47] on the gaseous adsorption of hydrogen, the hydrogen adsorption per molecule of platinum was shown to be 2 to 5 times higher than that of gold at similar conditions.[47] In the adsorption pseudo-capacitance context, this parameter is reflected as a constant ($q_{max}$) representing the charge required to reach maximum coverage by $H_{ads}$, as discussed by Conway and Tilak:[41]

$$C_F = \frac{dq}{dE} = q_{max}\frac{d\theta}{dE}$$

Therefore, considering the smaller number of available active sites on gold (lower $q_{max}$), as compared to more active metals such as platinum[47] and palladium,[48] it is reasonable to expect significantly lower adsorption pseudo-capacitance, for the same magnitude of the surface coverage (θ). This makes it difficult to use the adsorption pseudo-capacitance as an unambiguous measure of surface coverage (θ) across different metals.

Another parameter that affects the observed adsorption pseudo-capacitance is $u$, the interaction coefficient of $H_{ads}$. That is, higher interaction amongst adsorbed hydrogen atoms results in lower maximum coverage by $H_{ads}$. This effect was discussed in detail in a study by Conway and Gileadi.[5] They demonstrated that increasing $u$ from 0 to 20 decreased the adsorption pseudo-capacitance by more than one order of magnitude at $\theta = 0.5$. This effect may be considered significant as the Volmer-Tafel mechanism also suggested the value of $u$ to be in the higher range discussed by Conway and Gileadi.[5] Therefore, one can argue that the adsorption pseudo-capacitance on a gold surface can be lower than what would be observed on active surfaces like platinum by a few orders of magnitude, at the same value of θ.

On the other hand, in a series of studies using phase-shift method to investigate the electro-adsorption of hydrogen atoms on various metals,[6,7,49] Chun et al. reported a Langmuir isotherm to describe the adsorption of hydrogen on polycrystalline gold surface.[6] Their measurements showed a low surface coverage at the low cathodic overpotentials, which was rapidly increased to full coverage at higher cathodic overpotentials. Based on these results, authors report the value of $K = 2.3 \times 10^{-6}$ $M^{-1}$ for the Langmuir equilibrium constant.[6] The results reported in that study are well compatible with the HER mechanism that includes a surface diffusion rate determining step at $\theta \rightarrow 0$ over low current densities and a Heyrovsky rate determining step at $\theta \rightarrow 1$ over high current densities.

Furthermore, in studies on the chemisorption of hydrogen on gold surfaces, it was frequently reported that the low coordinated gold atoms at corner and edge positions in the crystal lattice have significantly higher activity in adsorption and dissociation of molecular hydrogen.[50–53] In a density functional theory study of $H_2$

dissociation on gold clusters, Barrio et al.[54] showed that some of the low coordination gold atoms can actively dissociate the H-H bound without any significant activation energy barrier. Since the catalytic behavior would enhance both directions of a reaction, the revers reaction, which is essentially the Tafel recombination step, is expected to proceed with a minimal activation energy barrier as well. These findings are in agreement with the surface diffusion mechanism, in a sense that they suggest distinct –but scarce– reaction sites at the gold surface with particularly higher activity for the Tafel recombination step. Similar significant structural dependent reaction rates for the HER was also reported for other materials such as $MoS_2$, as reviewed in more detail elsewhere.[55]

Overall, considering the extent of hydrogen adsorption on a gold surface as a differentiating criterium, the mechanism including a surface diffusion as a rate determining step is a better representative of the electrochemical behavior of the HER than the mechanism based on Tafel rate determining step. Therefore, considering the results and discussion in the present section, a modified mechanism for the HER can be proposed as Reaction 12 to Reaction 15.

$$H^+ + e^- \rightleftharpoons H_{ads,A} \quad [12]$$

$$H_{ads,A} \rightarrow H_{ads,B} \quad [13]$$

$$2\,H_{ads,B} \rightarrow H_2 \quad [14]$$

$$H_{ads,A\ or\ B} + H^+ + e^- \rightarrow H_2 \quad [15]$$

In the reactions above, subscripts *A* represents majority of the reaction sites that are placed at the plane gold surface, and *B* represent a small fraction of the surface with significantly higher activity for the Tafel reaction (as compared to sites *A*). Reaction 13 represents the surface diffusion step preceding the Tafel reaction, which may be limiting the overall rate of the Tafel reaction a result of the low mobility of $H_{ads}$, or perhaps because of the scarcity of B sites. On the other hand, as suggested in Reaction 15, the Heyrovsky reaction may occur at both sites A and B.

## Mathematical Model

While the arguments based on a parametric study, such as the one in previous section, provide some insight into the underling mechanisms, they cannot properly reflect the complex relationship between pH, potential, *K*, *u*, surface coverage, as well as the mass transfer effect. This issue may be addressed by implementing a more comprehensive mathematical treatment. In the following, a mathematical model of the HER on a rotating disk electrode (RDE) was developed, and used to examine whether the mechanism proposed in Discussion section was able to properly describe the behavior of the HER across the pH and potential range of the present study.[a]

In order to calculate the rate of electrochemical reactions, the surface hydrogen ion concentration [$H^+$] appearing in the reaction rate relationships (Equation 5 and Equation 6) needs to be specified. However, the surface concentration of an electro-active species can significantly differ from its bulk concentration due to mass transfer limitation. This can be particularly pronounced during the measurements when the electrode is polarized more negatively and the cathodic reaction rate becomes mass transfer controlled. The surface concentration of hydrogen ions can be calculated by solving the mass conservation equation throughout the diffusion boundary layer. The mass conservation equation for species *i* includes the transport of the species due to molecular diffusion, electromigration and laminar convection, as described by the Nernst-Planck equation:[56]

$$\frac{\partial C_i}{\partial t} = -\nabla . N_i + R_i \quad [16]$$

Where $R_i$ describes the homogeneous chemical reactions including species *i* and:

$$N_i = -z_i U_i F C_i \nabla\phi - D_i \nabla C_i + \upsilon C_i \quad [17]$$

Assuming a steady state condition ($\partial C_i/\partial t = 0$), a one-dimensional semi-infinite geometry in the direction *x* normal to the RDE electrode surface and an infinitely diluted solution, Equation 16 can be restated as:

$$0 = -D_i \frac{\partial}{\partial x}\frac{\partial C_i}{\partial x} - \frac{\partial}{\partial x}\left(\frac{z_i D_i F C_i}{RT}\frac{\partial \phi}{\partial x}\right) + \upsilon_x \frac{\partial C_i}{\partial x} + R_i \quad [18]$$

The convective flow component in direction *x* for a RDE electrode was described as:[57]

$$\upsilon_x = -a\Omega\left(\frac{\Omega}{\nu}\right)^{1/2} x^2 \quad [19]$$

where $a = 0.510$ and the diffusion layer thickness (δ) was:[57]

$$\delta = \left(\frac{3D_{H+}}{a\nu}\right)^{1/3}\left(\frac{\Omega}{\nu}\right)^{-1/2} \quad [20]$$

The only homogeneous chemical reaction in the present study is the water dissociation as shown in Reaction 21, which was mathematically described by Equation 22 where $i = H^+$ or $OH^-$. The values for reaction rate constant of water dissociation and recombination, $k_{f,w}$ and $k_{b,w}$, can be found in an earlier study.[28]

$$H_2O_{(l)} \leftrightharpoons OH^-_{(aq)} + H^+_{(aq)} \quad [21]$$

$$R_i = k_{f,w} - k_{b,w}\left[H^+\right]\left[OH^-\right] \quad [22]$$

Equation 18 was applied for each species *i* in the system (i.e. $H^+$, $OH^-$, $Na^+$, $ClO_4^-$). The electric potential (ϕ) in the solution appearing in the electromigration term can be calculated so that the electroneutrality constraint is satisfied:

$$\sum_i z_i C_i = 0 \quad [23]$$

The second order differential transport equations (such as Equation 18) requires two sets of boundary conditions. The boundary condition at the bulk solution is a known and constant concentration of the chemical species. Also, the potential at the bulk is considered to be a constant arbitrary number (zero) serving merely as a reference value.

At the electrode/solution interface, the boundary conditions are dictated by the fluxes of species due to the electrochemical reactions, which are defined by the reaction mechanism. The flux at the electrode surface for an electroactive species *i* is defined as:

$$N_i = -\sum_j s_{ij}\upsilon_j \quad [24]$$

This equation assumes that species *i* can be involved in *j* electrochemical reactions at the surface. In the system considered here, the only electroactive species is the hydrogen ion, where the reaction rates for this species are described by Equation 5 and Equation 6.

The surface flux of non-electroactive species is zero:

$$N_i = 0 \quad [25]$$

Finally, the surface coverage of the adsorbed hydrogen atoms (θ) appearing in the electrochemical reaction rates needs to be accounted for. The surface coverage can be calculated by mass conservation using the rate expressions, assuming a steady state condition:

$$\frac{d\theta_A}{dt} = \upsilon_V - \upsilon_{H,A} - \upsilon_D = 0 \quad [26]$$

[a]The source code of the mathematical model and the parametric study can be provided upon request.

**Table III. Summary of equations used in the mathematical model.**

| | |
|---|---|
| Electrode surface boundary | |
| $N_i = -\sum_j s_{ij}\upsilon_j$ | *electro active species* |
| $N_i = 0$ | *non − electro active species* |
| $\sum_i z_i C_i = 0$ | |
| $\frac{d\theta_A}{dt} = \upsilon_V - \upsilon_{H,A} - \upsilon_D = 0$ | |
| $\frac{d\theta_B}{dt} = \upsilon_D - \upsilon_{H,B} - 2\upsilon_T = 0$ | |
| Diffusion layer | |
| $-D_i\frac{\partial}{\partial x}\frac{\partial C_i}{\partial x} - \frac{\partial}{\partial x}\left(\frac{z_i D_i F C_i}{RT}\frac{\partial \phi}{\partial x}\right) + \upsilon_x\frac{\partial C_i}{\partial x} = 0$ | *all species* |
| $\sum_i z_i C_i = 0$ | |
| Bulk boundary conditions | |
| $C_i = C_i^b$ | *all species* |
| $\phi = 0$ | |

$$\frac{d\theta_B}{dt} = \upsilon_D - \upsilon_{H,B} - 2\upsilon_T = 0 \qquad [27]$$

All the governing equations and boundary conditions implemented in the model are summarized in Table III. These equations form a set of seven nonlinear, coupled, differential equations which were solved (as described in Methodology section) to obtain the values of the seven unknowns: four aqueous concentrations for $H^+$, $OH^-$, $Na^+$ and $ClO_4^-$ ions, potential inside the diffusion layer, and the surface coverage by the adsorbed hydrogen atoms at sites A and B.

***Model verification.***—The simulations of the current potential behavior for the present system were done with the following assumptions:

- The desorption of $H_{ads,A}$ due to Tafel reaction was negligible.
- Both $H_{ads,A}$ and $H_{ads,B}$ were involved in Heyrovsky reaction.
- The effect of $H_{ads,B}$ interaction ($u\theta_B$) was assumed to be negligible considering $\theta_B \rightarrow 0$.

The symmetry factors ($\beta$ *and* $\lambda$) were taken to be 0.5 and the reaction rate constants of the elementary steps, $K$, and $u$ were used as adjustable parameters. The following set of parameters resulted in the best fit of the model by simultaneously considering the experimental polarization curves at all pH values: $K = 3.3 \times 10^{-7}\ M^{-1}$, $u = 2.3$, $k_{f,V} = 4 \times 10^{-6}$ ($^m/_s$), $k_{f,H} = 1.2 \times 10^{-10}$ ($\frac{m^3}{mol.s}$), $k_{f,T} = 2.5 \times 10^{-2}$ ($\frac{m^2}{mol.s}$), $k_{f,D} = 3.5 \times 10^{-6}$ ($\frac{m^2}{mol.s}$).

Figure 7 shows the comparison of the simulated results with the experimental data. The simulated voltammograms showed a very good agreement with experimental results over the lower Tafel slope range, while the transition to the higher Tafel slope of ~120 mV was also predicted reasonably well. The apparent reaction order of 0.81 observed at −0.41 V (vs. SHE) in Figure 7 also agreed well with the experimental data as reported in Figure 2.

The calculated change of $H_{ads}$ coverage during polarization for both sites A and B are demonstrated in Figure 8 for pH 2. These results were also found to agree well with what was suggested by the parametric study. As shown in Figure 8, the coverage at B (desorption) sites was negligibly small throughout the whole current density range. On the other hand, the coverage at A (adsorption) sites was low in the ~60 mV Tafel slope range, while at higher current densities the surface was almost fully covered with $H_{ads,A}$. The plateau at the high surface coverage range coincides with the change of the mechanism from surface diffusion controlled to Volmer-Heyrovsky control at high cathodic current densities resulting in the observed ~120 mV Tafel slope (Figure 3 and Figure 4).

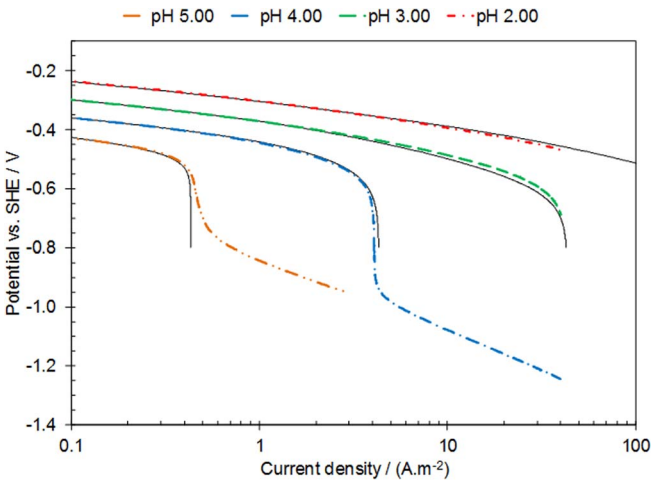


**Figure 7.** Comparison of the linear sweep voltammograms obtained experimentally and the results from the model at 2000 rpm, 30°C and 0.1 M $NaClO_4$.

The contribution of each reaction route to the net current density is demonstrated in Figure 9. This graph suggests that the Volmer-Heyrovsky route does not have any significant contribution at low current densities and it becomes significant only at high current densities and low pH values. The predicted results at pH 0 suggest that in a more acidic environment a mixed controlled mechanism may be observed. Considering the Tafel slope (~40 mV) and reaction order of 2 for the Heyrovsky reaction at such surface conditions (Figure 4), one can expect to observe a slight decrease in Tafel slope and increase in reaction order when compared to higher pH values.

## Conclusions

The mechanism and the kinetics of the HER was studied in acidic perchlorate solutions with an extended pH range up to pH 5. The existing mechanisms were reevaluated and shown to be inadequate in explaining the steady state polarization behavior of the hydrogen evolution reaction over extended cathodic potential range and a broad range of acidic pH values.

The experimental data obtained in the present study for hydrogen evolution on gold in mild perchloric acid solutions showed two distinctive Tafel slopes of 68 ± 5 mV and 120 ± 2 mV at lower and higher current densities, respectively. At the experimental conditions

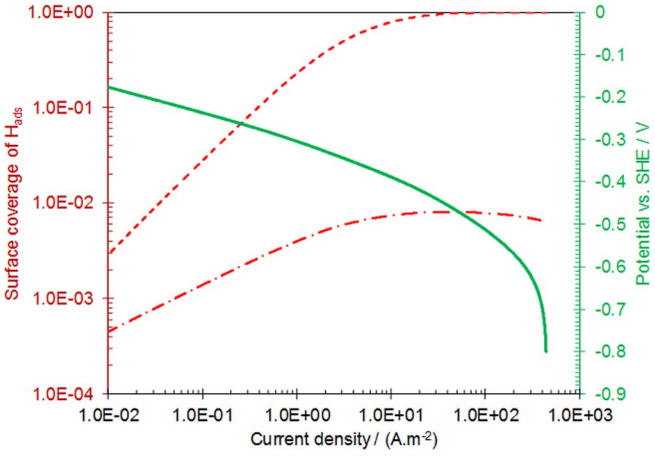


**Figure 8.** The calculated surface coverage of $H_{ads,A}$ (dashed red line on the primary vertical axis), $H_{ads,B}$ (dotted-dashed red line on the primary vertical axis), and polarization curve (solid green line on the secondary vertical axis) at pH 2, 2000 rpm, 30°C and 0.1 M $NaClO_4$.

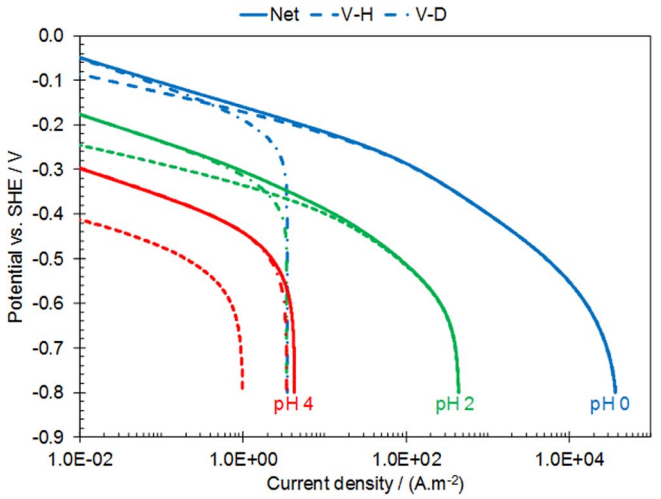


**Figure 9.** Current densities corresponding to each reaction pathway. Solid lines are the net currents, dashed lines represent the contribution of the Volmer-Heyrovsky route and dotted dash line represents the contribution of the surface diffusion route (followed by Tafel desorption step) at pH 4 (red), pH 2 (green), and pH 0 (blue).

of the present work, the higher Tafel slope was only observed at pH values below 3. At the same time, the apparent reaction order of the HER in the pH range from 2 to 5, was found to be approximately 0.8.

The plausible mechanisms based on the conventional Volmer, Tafel, and Heyrovsky elementary steps, as well as the mechanisms including a surface diffusion step, were analyzed via a parametric study of the kinetic parameters. The results suggests that the polarization behavior of HER on gold over an extended pH range was explained best when a surface diffusion step preceding the Tafel recombination reaction was considered, along with the previously known elementary steps. This diffusion step was further discussed and found to be in agreement with the atomistic level studies on adsorption and dissociation of hydrogen gas on gold surfaces.

The proposed mechanism suggests that at low current densities, the rate of the HER was limited by the surface diffusion of $H_{ads}$, regardless of the solution pH. At higher current densities and in more acidic solutions, where a 120 mV Tafel slopes were observed, the rate limiting step was the slow electrochemical desorption reaction (Heyrovsky step). This proposed mechanism was incorporated into a comprehensive mathematical model. The simulated polarization curves showed a reasonable agreement with both the lower and the higher Tafel slopes as well as the apparent reaction order, further supporting the proposed mechanism.

## Acknowledgments

The authors acknowledge the financial support from Anadarko, Baker Hughes, BP, Chevron, China National Offshore Oil Corporation, CNPC Tubular Goods Research Center, ConocoPhillips, DNV GL, ExxonMobil, M-I SWACO, Occidental Oil Company, Petroleum Institute, PTT, Saudi Aramco, Shell Global Solutions, SINOPEC, TOTAL, TransCanada, and WGK under a joint industrial research project. The authors are also grateful for constructive comments and discussions with Dr. D. Young, Ohio University.

## List of Symbols

| | |
|---|---|
| b | Tafel slope (mV) |
| $C_i$ | Concentration of species $i$ ($mol.m^{-3}$) |
| $C_F$ | Faradic capacitance ($F.m^{-2}$) |
| $D_i$ | Diffusion coefficient of species $i$ ($m^2.s^{-1}$) |
| $E$ | Applied potential (V) |
| $F$ | Faraday's constant ($C.mol^{-1}$) |
| $i$ | Current density ($A.m^{-2}$) |
| $K$ | Equilibrium constant of the Volmer reaction ($M^{-1}$) |
| $k_{f,j}$ | Forward reaction rate constant of reaction j |
| $k_{b,j}$ | backward reaction rate constant of reaction j |
| $N_i$ | Flux of species $i$ ($mol.m^{-2}.s$) |
| $p_{(H^+)}$ | Reaction order with respect to $H^+$ concentration |
| $q$ | Charge required for surface coverage of θ ($C.m^{-2}$) |
| $q_{max}$ | Charge required for θ = 1 ($C.m^{-2}$) |
| $R$ | Universal gas constant ($J.mol^{-1}.K^{-1}$) |
| $R_i$ | Rate of homogeneous reaction $i$ ($mol.s^{-1}.m^{-3}$) |
| $s_{ij}$ | Stoichiometric coefficient of species $i$ in reaction $j$ |
| $T$ | Absolute temperature (K) |
| $t$ | Time (s) |
| $u$ | Correlation coefficient of $H_{ads}$ interaction energy, defined as $u = \frac{(\partial \Delta G^o_{ads}/\partial \theta)}{RT}$ where $\partial \Delta G^o_{ads}$ is the standard Gibbs free energy of adsorption. |
| $U_i$ | Mobility of species $i$ ($m.s^{-1}$) |
| $v$ | Velocity ($m.s^{-1}$) |
| $x$ | Spatial dimension (m) |
| $z_i$ | Charge of species i |

### Greek

| | |
|---|---|
| $\beta_j$ | Electrochemical symmetry factor of reaction j |
| δ | Diffusion layer thickness of RDE |
| $\xi_i$ | Dimensionless concentration of species $i$ |
| ϕ | Potential in the electrolyte (V) |
| Φ | Dimensionless potential in the electrolyte |
| $\lambda_j$ | Symmetry factor of reaction j due to interaction of adsorbed species |
| ν | Kinematic viscosity ($m^2.s^{-1}$) |
| Ω | Rotation speed ($rad.s^{-1}$) |
| Ψ | Dimensionless applied potential |
| θ | Surface coverage of $H_{ads}$ |
| $\upsilon_j$ | Reaction rate of reaction j ($mol.m^{-2}.s^{-1}$) |
| ζ | Dimensionless spatial dimension |

## References

1. E. Santos, a. Lundin, K. Pötting, P. Quaino, and W. Schmickler, *Phys. Rev. B - Condens. Matter Mater. Phys.*, **79**, 1 (2009).
2. M. Jafarian, M. Behazin, I. Danaee, and F. Gobal, *Res. J. Chem. Sci.*, **3**, 56 (2013).
3. L. A. Khanova and L. I. Krishtalik, *J. Electroanal. Chem.*, **660**, 224 (2011).
4. B. E. Conway and M. Salomon, *Electrochim. Acta*, **9**, 1599 (1964).
5. B. E. Conway and E. Gileadi, *Trans. Faraday Soc.*, **58**, 2493 (1962).
6. J. H. Chun, K. H. Ra, and N. Y. Kim, *J. Electrochem. Soc.*, **150**, E207 (2003).
7. J. H. Chun, S. K. Jeon, N. Y. Kim, and J. Y. Chun, *Int. J. Hydrogen Energy*, **30**, 1423 (2005).
8. A. Hamelin, L. Stoicoviciu, S. -C. Chang, and M. J. Weaver, *J. Electroanal. Chem. Interfacial Electrochem.*, **307**, 183 (1991).
9. F. Safizadeh, E. Ghali, and G. Houlachi, *Int. J. Hydrogen Energy*, **40**, 256 (2015).
10. A. Lasia, in *Handbook of Fuel Cells*, (2010).
11. N. M. Markovic and P. N. J. Ross, *Surf. Sci. Reports*, **45**, 117 (2002).
12. M. Balat, *Int. J. Hydrogen Energy*, **33**, 4013 (2008).
13. L. A. Khanova and L. I. Krishtalik, *J. Electroanal. Chem.*, **660**, 224 (2011).
14. N. Pentland, J. O. Bockris, and E. Sheldon, *J. Electrochem. Soc.*, **104**, 182 (1957).
15. G. J. Brug, M. Sluyters-Rehbach, J. H. Sluyters, and A. Hemelin, *J. Electroanal. Chem.*, **181**, 245 (1984).
16. J. Perez, E. ., R. Gonzalez, and H. M. Villullas, *J. Phys. Chem. B*, **102**, 10931 (1998).
17. B. E. Conway and L. Bai, *Electrochim. Acta*, **31**, 1013 (1986).
18. A. T. Kuhn and M. Byrne, *Electrochim. Acta*, **16**, 391 (1971).
19. P. J. Hillson, *Trans. Faraday Soc.*, **48**, 462 (1952).
20. D. J. G. Ives, *Can. J. Chem.*, **37**, 213 (1959).
21. R. Parsons, G. Picq, and P. Vennereau, *J. Electroanal. Chem.*, **181**, 281 (1984).
22. G. J. Brug, M. Sluyters-Rehbach, J. H. Sluyters, and A. Hemelin, *J. Electroanal. Chem.*, **181**, 245 (1984).
23. J. O. Bockris, I. A. Ammar, and A. K. M. S. Huq, *J. Phys. Chem.*, **61**, 879 (1957).
24. L. I. Krishtalik, *Electrochim. Acta*, **48**, 181 (2002).
25. A. Hamelin, *J. Electroanal. Chem.*, **386**, 1 (1995).
26. D. D. Bode Jr., T. N. Andersen, and H. Eyring, *The Journal of Physical Chemistry*, **71**, 792 (1967).
27. A. Kahyarian, B. Brown, and S. Nesic, *Corrosion*, **72**, 1539 (2016).
28. A. Kahyarian, M. Singer, and S. Nesic, *J. Nat. Gas Sci. Eng.*, **29**, 530 (2016).
29. M. B. Kermani and A. Morshed, *Corrosion*, **59**, 659 (2003).

30. M. Nordsveen, S. Nešić, R. Nyborg, and A. Stangeland, *Corrosion*, **59**, 443 (2003).
31. S. Nešić, J. Postlethwaite, and S. Olsen, *Corrosion*, **52**, 280 (1996).
32. L. G. S. Gray, B. G. Anderson, M. J. Danysh, and P. R. Tremaine, in *Nace International*, Paper No. 464 (1989).
33. F. M. Song, *Electrochim. Acta*, **55**, 689 (2010).
34. J. O. Bockris and D. F. A. Koch, *J. Phys. Chem.*, **65**, 1941 (1961).
35. J. O. Bockris, J. McBreen, and L. Nanis, *J. Electrochem. Soc.*, **112**, 1025 (1965).
36. W. Sheng, H. A. Gasteiger, and Y. Shao-Horn, *J. Electrochem. Soc.*, **157**, B1529 (2010).
37. S. Schuldiner, *J. Electrochem. Soc.*, **101**, 426 (1954).
38. N. T. Thomas and K. Nobe, *J. Electrochem. Soc.*, **117**, 622 (1970).
39. S. Schuldiner, *J. Electrochem. Soc.*, **108**, 384 (1961).
40. S. Schuldiner, *J. Electrochem. Soc.*, **101**, 426 (1954).
41. B. E. Conway and B. V. Tilak, *Electrochim. Acta*, **47**, 3571 (2002).
42. J. O. Bockris and E. C. Potter, *J. Electrochem. Soc.*, **99**, 169 (1952).
43. J. O. Bockris and A. K. N. Reddy, *Modern Electrochemistry: An introduction to an interdisiplinary area*, Volume **2**, Plenum Press, New york, (1973).
44. M. Enyo, *J. reasearch Inst. Catal.*, **25**, 17 (1977).
45. M. R. Gennero de Chialvo and A. C. Chialvo, *Electrochim. Acta*, **44**, 841 (1998).
46. M. R. Gennero de Chialvo and A. C. Chialvo, *Electrochem. commun.*, **1**, 379 (1999).
47. E. Bus and J. A. van Bokhoven, *Phys. Chem. Chem. Phys.*, **9**, 2894 (2007).
48. M. Łukaszewski, K. Kuśmierczyk, J. Kotowski, H. Siwek, and A. Czerwiński, *J. Solid State Electrochem.*, **7**, 69 (2003).
49. J. H. Chun and N. Y. Kim, *Int. J. Hydrogen Energy*, **31**, 277 (2006).
50. L. Stobiński, L. Zommer, and R. Duś, *Appl. Surf. Sci.*, **141**, 319 (1999).
51. M. Casarin, C. Maccato, and A. Vittadini, *J. Phys. Chem. B*, **106**, 795 (2002).
52. L. Stobinski, R. Nowakowski, and R. Dus, *Vacuum*, **48**, 203 (1997).
53. M. Hu, D. P. Linder, M. B. Nardelli, and A. Striolo, *J. Phys. Chem. C*, **117**, 15050 (2013).
54. L. Barrio, P. Liu, J. A. Rodríguez, J. M. Campos-Martín, and J. L. G. Fierro, *J. Chem. Phys.*, **125** (2006).
55. Y. Zheng, Y. Jiao, M. Jaroniec, and S. Z. Qiao, *Angew. Chemie - Int. Ed.*, **54**, 52 (2015).
56. J. Newman and K. E. Thomas-Alyea, *Electrochemical Systems*, 3rd ed., Wiley-interscience, (2004).
57. W. G. Cochran, *Math. Proc. Cambridge Philos. Soc.*, **1**, 365 (1934).
58. J. Newman, *Ind. Eng. Chem. Fundam.*, **7**, 514 (1968).
59. J. S. Newman, *Electrochemical systems*, 1st ed., Prentice hall, Inc., (1973).
60. M. J. Mader, C. W. Walton, and R. E. White, *J. Electrochem. Soc.*, **133**, 1124 (1986).
61. T. V. Nguyen, C. W. Walton, and R. E. White, *J. Electrochem. Soc.*, **133**, 1130 (1986).
62. K. -M. Yin, T. Yeu, and R. W. White, *J. Electrochem. Soc.*, **138**, 1051 (1991).
63. D. H. Coleman, R. E. White, and D. T. Hobbs, *J. Electrochem. Soc.*, **142**, 1152 (1995).
64. M. Ramasubramanian, *J. Electrochem. Soc.*, **146**, 111 (1999).